ACS APPLIED MATERIALS & INTERFACES

www.acsami.org

Research Article

Oxygen Plasma-Mediated Microstructured Hydrocarbon Membrane for Improving Interface Adhesion and Mass Transport in Polymer Electrolyte Fuel Cells

Jiwoo Choi,[○] Dongsu Kim,[○] Ji Eon Chae,[○] Sanghyeok Lee, Sang Moon Kim, Sung Jong Yoo, Hyoung-Juhn Kim,* Mansoo Choi,* and Segeun Jang*

Cite This: https://doi.org/10.1021/acsami.2c15122

Read Online

ACCESS | Metrics & More | Article Recommendations | Supporting Information

ABSTRACT: Developing a method for fabricating high-efficient and low-cost fuel cells is imperative for commercializing polymer electrolyte membrane (PEM) fuel cells (FCs). This study introduces a mechanical and chemical modification technique using the oxygen plasma irradiation process for hydrocarbon-based (HC) PEM. The oxygen functional groups were introduced on the HC-PEM surface through the plasma process in the controlled area, and microsized structures were formed. The modified membrane was incorporated with plasma-treated electrodes, improving the adhesive force between the HC-PEM and the electrode. The decal transfer was enabled at low temperatures and pressures, and the interfacial resistance in the membrane−electrode assembly (MEA) was reduced. Furthermore, the micropillar structured electrode configuration significantly reduced the oxygen transport resistance in the MEA. Various diagnostic techniques were conducted to find out the effects of the membrane surface modification, interface adhesion, and mass transport, such as physical characterizations, mechanical stress tests, and diverse electrochemical measurements.

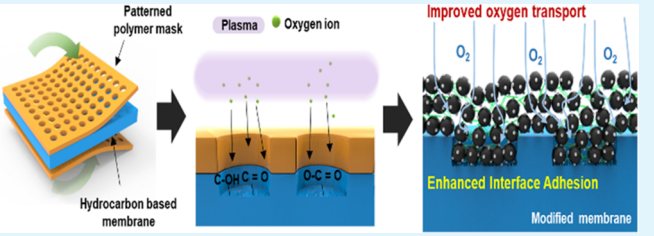

KEYWORDS: *fuel cell, hydrocarbon membrane, plasma, microstructure, adhesion, mass transport*

1. INTRODUCTION

Polymer electrolyte membrane (PEM) fuel cells (FCs) have been in the spotlight as next-generation energy sources due to their high-energy conversion efficiency and zero-emission operation. Over the past few decades, intensive research has been conducted to fabricate a highly efficient membrane−electrode assembly (MEA), allowing technical maturity to reach commercialization. However, many challenges must be solved for successful commercialization, such as the long-term stability and system cost of PEMFC.[1−4] Because expensive catalysts and membranes are needed currently for manufacturing MEA, the capital cost of PEMFCs is not yet competitive in the market. It is far below the Department of Energy's system cost target of \$30 kW^{-1}.[5] Among the expensive materials for MEA, perfluorosulfonic acid (PFSA) is the most widely used proton conductive polymer due to its high conductivity, chemical stability, and mechanical robustness. However, the fluorinating process for the fabrication of the membrane causes environmental problems and a high material cost of \$500 m^{-2} or more (for commercially available Nafion membranes), and the high gas permeability of the membrane causes the chemical degradation of MEA.[6,7]

Great efforts have been made to develop cheaper membranes with superior membrane properties to commercial PFSAs. Primarily, nonfluorinated hydrocarbon-based (HC) PEMs have been widely studied.[8−12] These HC-PEMs are promising electrolyte materials with several advantages, such as low gas permeability, excellent thermal stability, and physical properties.[13] Typically, HC-PEMs are based on readily available and inexpensive materials. Also, the eco-friendly synthesis process of HC-PEMs has the advantage of reducing production costs by eliminating fluorinating steps. Therefore, HC-PEMs are noteworthy as cost-effective cation-exchange membranes to replace high-cost PFSA-PEMs, such as Nafion, Flemion, and Aciplex.[1,14] For application to PEMFCs, HC-PEM is incorporated into MEA with PFSA ionomer-containing catalyst layers (CLs). However, poor compatibility and adhesion due to different chemical properties of HC and PFSA polymers causes interfacial issues between them, eventually weakening their performance and durability.[15]

Therefore, several efforts have been made to improve the compatibility between the HC-PEM and PFSA-CL chemically or mechanically. For example, chemical modification ap-

Received: August 23, 2022
Accepted: October 25, 2022

proaches, such as synthesizing partially fluorinated HC-PEM,[16−18] employing HC-ionomer in CL,[15,19,20] and introducing an interfacial adhesion layer based on a PFSA ionomer,[21,22] were reported. Jeong et al. developed the interface adhesion layer approach by forming the layer with mixed HC and PFSA ionomers with gradient compositions, improving the interfacial bonding strength and stability between HC-PEM and PFSA-CL.[21] Regarding the mechanical modification approach, introducing micro-/nanostructures or roughness at the interface has achieved a mechanical fastener effect from interlocked geometry.[23−25] Recently, Oh et al. introduced solvent vapor and partially dissolved the HC membrane. The solvent-vapor-induced interface modifying method impregnated the membrane into cathode CLs, enlarging the electrochemical surface area and reducing interfacial resistance.[23] However, most approaches require newly synthesized materials or complicated processes using high-boiling-point solvents not easily applicable to the membrane dual-side modification approach and need a post-treatment process to remove residual solvent. Therefore, there is a great need for a new strategy that can be easily applied to the commercial MEA manufacturing process (e.g., the decal transfer method) while improving interfacial adhesion and system performance.

This study introduces a combined mechanical and chemical strategy for enhancing the HC-PEM/CL interface of PEMFC using a spatially controlled oxygen plasma irradiation method. Microsized holes and oxygen functional groups were successfully introduced onto the HC membrane's surface through an oxygen plasma-etching process using a polymer stencil with regular openings. The modified membrane was easily incorporated with oxygen plasma-treated electrodes using a low-temperature and low-pressure decal transfer method due to enhanced interface adhesion force. By mechanical bonding and shear force measurements, the microsized structures in the HC-PEM and the chemical functional group on its surface were found to improve the bonding strength between HC-PEM and PFSA polymers. Also, the modified MEA showed significantly improved power density with decreased Ohmic and mass-transport resistances. By applying a transmission line model, the improved bonding strength prevented exfoliation of the electrode from the membrane and reduced Ohmic and proton transport resistances at the interface. Furthermore, a detailed analysis of the limiting current density verified that the modified MEA showed remarkably reduced oxygen transport resistance within the electrode because of the micropillar structure inducing a highly porous electrode array region, functioning as an oxygen transport highway.

2. EXPERIMENTAL SECTION

2.1. Preparing an HC-Based Membrane. Sulfonated poly (arylene ether sulfone) with 40% disulfonate (BPSH-40) (Aquafone, YANJIN Technology, China) was prepared for a 10 wt % polymer solution in dimethylacetamide. The polymer solution was filtered using a 0.45 μm Teflon syringe filter. The solution was cast on a glass plate and dried in a vacuum oven to remove the solvent.

2.2. Constructing a Polymeric Stencil Mask with Microsized Apertures. The fabrication process of a polymeric stencil has been described in detail in the previous paper[26] and is summarized here. First, to prepare a polydimethylsiloxane (PDMS) mold with microsized pillar arrays (diameter 20 μm), a curing agent and base (Sylgard 184 kit, Dow Corning) were mixed in a weight ratio of 1:10 and poured onto the prepared silicon master with microsized holes (diameter 20 μm) and cured at 80 °C for 1 h. A flat PDMS mold was prepared similarly on a flat silicon master. Next, 100 μl of ultraviolet (UV)-curable polyurethane acrylate (PUA, 311RM) resin (Changsung sheet, Korea) was applied between the patterned PDMS and the flat PDMS, and the assembly was gently pressed. The assembly was cured using a UV cure system (Minuta technology, Korea) for ∼1 min, at 15 W cm^{-2}. Oxygen permeation through gas-permeable PDMS molds inhibits free-radical polymerization by scavenging initiator radicals at the interface between flat and pillared structures. Therefore, a thin polymeric film with a uniform 20-μm-sized aperture array was fabricated, and the polymeric stencil was further cured for 1 h for complete curing.

2.3. Simultaneous Chemical and Mechanical Modification Process. A conformal contact with the membrane was formed by laminating the prepared stencil thermally on the HC membrane at a pressure of 5 MPa at 80 °C. To selectively etch the membrane, the assembly was kept in a vacuum plasma chamber (Femto Science, Korea). During the process, the pressure was maintained at ∼4.5 × 10^{-1} torr working pressure, with an oxygen flow rate of 20 sccm, a frequency of 50 kHz, and a power of 100 W. In this study, the etching rate was carefully controlled at 0.068−0.075 μm min^{-1}. Due to the polymeric stencil with regular openings, only the uncovered surface was etched to form a 20-μm-sized regular structure. Finally, the stencil was exfoliated, resulting in a mechanically and chemically modified HC-based membrane (MC-HC). To prepare a chemically modified membrane (C-HC) or additionally introduce oxygen functional groups to the electrode and MC-HC, the plasma process was performed for 2 min under a working pressure of ∼3.2 × 10^{-1} torr, an oxygen flow rate of 10 sccm, a frequency of 100 kHz, and a power of 25 W.

2.4. MEA Preparation. The prepared membrane (35 ± 2 μm thick) was treated with 1 M sulfuric acid (H_2SO_4) solution at 80 °C for 2 h, washed with distilled (DI) water for 1 h, and thoroughly dried. For preparing the CL, Pt/C (46.9 wt %, Tanaka) powder was dispersed in Nafion ionomer solution (5 wt %), isopropyl alcohol (IPA), DI water, and dipropylene glycol with an ionomer to carbon ratio of 0.8. After sufficiently dispersed by sonication, the slurry was bar-coated on a polyimide (PI) film, and the anode and cathode's catalyst loading were fixed to 0.2 mg cm^{-2}. The decal films were hot-pressed on both sides of the HC membrane at 140 °C for 5 min at a given pressure with an active area of 5 cm^2. In the case of C-HC and MC-HC, the plasma treatment process was conducted on the electrode and membrane surfaces before lamination. Finally, the PI film was detached from the MEA. The decal transfer yield was analyzed by examining the digitized image using ImageJ based on the residual electrode area ratio because the weight difference in the film before and after decal transfer was too small to measure quantitatively. After the transfer, the area fraction of the remaining electrodes in the upper and lower films were examined, and their average values were given.

2.5. Electrochemical Single-Cell Performance Analysis. The prepared MEAs were sandwiched between two gas diffusion layers (GDLs) (Sigracet 39BB, SGL Carbon, Germany), two Teflon gaskets (CNL Energy, Korea), and two graphite plates with a serpentine-type flow field. The single cell was assembled by fastening screws with a torque of ∼9 N m. A PEMFC test station (CNL Energy) and a potentiostat (BioLogic) were used to evaluate the single-cell performance. The cell temperature was 80 °C, and fully humidified hydrogen (150 sccm) and air (800 sccm) were supplied to the anode and cathode, respectively, to measure polarization curves and electrochemical impedance spectroscopy (EIS) spectra. The polarization curves were obtained using the current-sweep method with a scan rate of 50 mA cm^{-2}. The EIS was conducted at 0.6 V with an alternating current (AC) amplitude of 10 mV and a frequency of 100 mHz to 15 kHz. To analyze the MEA's catalyst usage, cyclic voltammetry (CV) was conducted with a sweeping range of 0.05−1.2 V and a scan rate of 50 mV s^{-1} by supplying fully humidified hydrogen (50 sccm) and nitrogen (200 sccm) to the anode and cathode, respectively. The hydrogen crossover-current density was measured using linear sweep voltammetry of 0.1−0.6 V under the

https://doi.org/10.1021/acsami.2c15122
ACS Appl. Mater. Interfaces XXXX, XXX, XXX−XXX

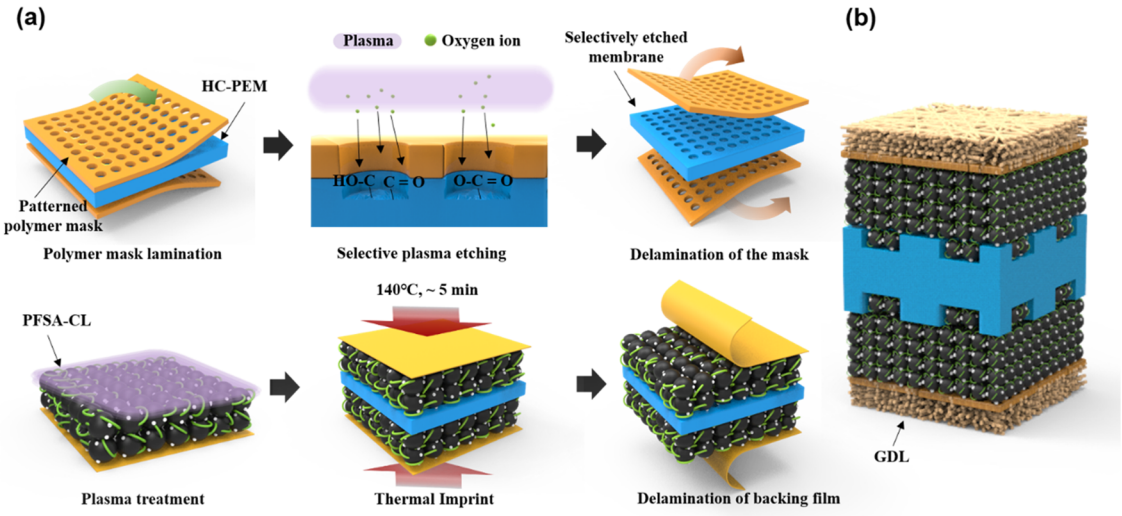

Figure 1. (a) Diagram of spatially controlled oxygen plasma irradiation and decal transfer processes of hydrocarbon-based (HC) polymer electrolyte membranes (PEM). (b) Schematic of a membrane−electrode assembly (MEA) with the modified HC-PEM.

condition of fully humidified hydrogen (anode, 200 sccm) and nitrogen (cathode, 200 sccm). Under the same environment, H_2/N_2 EIS was conducted to analyze the MEA's CL resistance at 0.2 V, with an AC amplitude of 5 mV and a frequency of 70 mHz to 100 kHz.

2.6. Oxygen Transport Resistance Measurement. The limiting current measurements for determining oxygen transport resistance were performed according to the oxygen concentration and gas pressure variance to analyze the oxygen transport resistance. The MEA fabrication procedures were consistent with the single-cell test. High flow rates of hydrogen (1000 sccm) and nitrogen-diluted oxygen (2000 sccm) were supplied to the anode and cathode, respectively. To avoid CL flooding, the relative humidity was controlled at 69%. The current density was recorded as the cell potential and decreased from 0.4 to 0.1 V with a 0.03 V interval, and the limiting current was chosen as the current density at 0.13 V. Oxygen mole concentrations of 0.5, 1, 1.5, and 2% were used, and the absolute pressures were 101, 151, 201, 251, and 301 kPa.

2.7. Physical and Chemical Characterizations. Field emission scanning electron microscopy (SEM) (JEOL, Japan) was used to obtain the surface and cross-sectional images of the membranes and MEAs. A contact angle analyzer (KRUSS, Germany) was used to measure the static water contact angle on the membranes. All of the tested samples were hot-pressed on the flat glass substrate to prevent the membranes from swelling. A universal testing machine (Instron, United States) was used to quantitatively compare the membranes' mechanical stability and the adhesion force between HC-based and PFSA membranes or CL. The stress−strain curves were measured for the Reference, C-HC, and MC-HC membranes of 1 × 4 cm^2. The peel-off strength was obtained for laminates of the Reference/Nafion, C-HC/Nafion, and MC-HC/Nafion. The prepared membranes (Reference, C-HC, and MC-HC) were laminated with a Nafion 212 (~50 μm, Dupont, United States) membrane at 10 MPa at 140 °C for 10 min, and the laminated area was controlled to 2 × 2 cm^2. The shear stress strength was obtained for the laminates of the Reference/CL/Nafion, C-HC/CL/Nafion, and MC-HC/CL/Nafion. The CL on the Nafion membrane was constructed by the hot-pressing with the decal film as same as the preparation of the MEA while keeping the area of 2 × 2 cm^2. Finally, the prepared CL/Nafion membrane was laminated with the prepared HC membrane under the same conditions as the peel-off test. When preparing the adhesion test samples, the Nafion and CL/Nafion membranes attached to the plasma-treated C-HC and MC-HC-PEMs were subjected to short plasma treatment before bonding. The water uptake and swelling ratios were determined in acid forms. All membranes were dried, and the weight (W_{dry}), length (l_{dry}), and thickness (t_{dry}) of the dry membranes were measured. The membranes were immersed in DI water for two days at 30 and 80 °C. After water immersion, the membranes were wiped lightly to remove the water droplets. The weight (W_{wet}), length (l_{wet}), and thickness (t_{wet}) of the swollen membranes were recorded. The water uptake and swelling ratios were calculated as follows:

$$\text{Water uptake } (\%) = \frac{(W_{wet} - W_{dry})}{W_{dry}} \times 100 \quad (1)$$

$$\text{Swelling ratio, } \Delta l = \frac{l_{wet} - l_{dry}}{l_{dry}} \times 100 \quad (2)$$

$$\text{Swelling ratio, } \Delta t = \frac{t_{wet} - t_{dry}}{t_{dry}} \times 100 \quad (3)$$

The membrane's proton conductivity was measured using the four-probe EIS. The membrane was prepared in 1 × 4 cm^2 and inserted into a conductivity cell with four Pt wire electrodes at 1 cm for each electrode. EIS measurements were conducted under a constant current of 0.1 mA, with an amplitude of 0.01 mA over 1 MHz to 1 Hz by supplying fully humidified nitrogen gas at 70 °C. The membranes' in-plane conductivities were calculated using the measured EIS resistance and the following equation:[27]

$$\sigma = \frac{L}{RA} \quad (4)$$

where L (cm), R (Ω), and A (cm^2) represent the distance between the electrodes, resistance of the membrane, and cross-sectional area of the membrane, respectively. The chemical states of the membranes were examined using X-ray photoelectron spectroscopy (XPS) (Kratos, United Kingdom).

3. RESULTS AND DISCUSSION

Figure 1a shows the fabrication process of a selectively plasma-etched membrane and MEA using a decal transfer method. First, a thin polymeric stencil with 20-μm-sized holes was prepared using PDMS with micropillar arrays, flat PDMS, and UV-curable polymer resin (fabrication details are explained in the Experimental Section and Figure S1). Then, the two polymeric stencils were attached to both sides of the HC-PEM, and the oxygen plasma-etching process was conducted only on the exposed surface of the HC-PEM, resulting in microsized holes and nanosized roughness. The etched hole's depth was carefully controlled by adjusting the etching time, and Figure

https://doi.org/10.1021/acsami.2c15122
ACS Appl. Mater. Interfaces XXXX, XXX, XXX−XXX

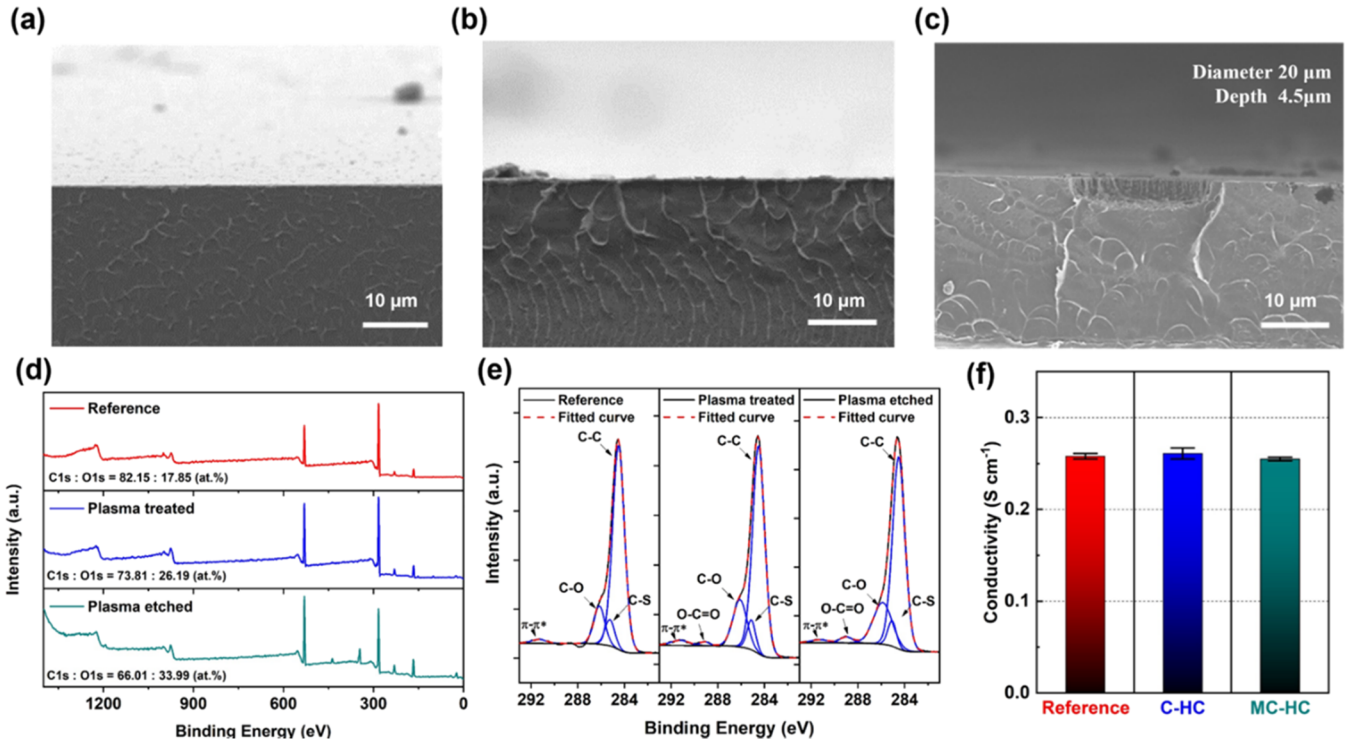

Figure 2. Cross-sectional scanning electron microscopy (SEM) images of the (a) Reference, (b) chemically modified hydrocarbon-based (HC) (C-HC), and (c) mechanically and chemically modified HC-based (MC-HC) membranes. (d) Wide-scan X-ray photoelectron spectroscopy (XPS) spectra and (e) C1s spectra of the reference, plasma-treated hydrocarbon-based (HC) polymer electrolyte membrane (PEM), and plasma-etched HC-PEM. (f) Proton conductivity of the reference, C-HC, and MC-HC membranes.

Table 1. Water Uptake and Swelling Ratios of the Reference, Chemically Modified Hydrocarbon (HC) (C-HC), and Mechanically and Chemically Modified HC-Based (MC-HC) Membranes

	water uptake (wt %)		swelling ratio (%)			
			Δl		Δt	
samples	30 °C	80 °C	30 °C	80 °C	30 °C	80 °C
reference	38.1 ± 1	45.1 ± 1.6	17.1 ± 1.4	21.7 ± 2.5	19.1 ± 2.1	22.7 ± 0.8
C-HC	44.5 ± 1.9	54.5 ± 2.2	16.7 ± 2.2	22 ± 1.2	21 ± 2.2	25.3 ± 3.3
MC-HC	44.9 ± 3.5	55.2 ± 2.1	16.7 ± 2.3	20.2 ± 1.7	21.4 ± 2.2	26.3 ± 2.9

S2 shows the linear relation between the etching time and the etched depth profile. This study selected the optimized etching depth as ∼4.5 μm by considering the transferred electrode thickness. This plasma-etching process was sequentially performed on each side surface, and the polymeric stencils were delaminated. After geometric modification, an ∼1 min plasma treatment was conducted on the entire surface of the modified membrane to introduce the oxygen functional groups on the HC-PEM's surface, including the intact surface. This process provides high surface energy to the membrane and creates binding sites. Next, to fabricate MEAs with improved interface adhesion between the modified HC-PEM and the CL, a decal transfer process was conducted by locating the modified HC-PEM between the short-time plasma-treated two CL/PI films under 140 °C at a given pressure. The PI films were carefully detached from the membrane, and finally, the MEA with the modified HC-PEM was prepared (Figure 1b).

The pristine and modified HC-PEMs with plasma treatment with/without etching were prepared to analyze the oxygen plasma effects mechanically and chemically on the HC-PEM surface. Figure 2a−c shows cross-sectional SEM images of the reference PEM (BPSH-40, the chemical structure is described in Figure S3), the C-HC by short-time plasma treatment, and the MC-HC with an etching thickness of ∼4.5 μm and a pattern diameter of 20 μm. The reference and plasma-treated membranes show a flat surface without geometrical modification, while the plasma-etched membrane shows microsized holes and nanosized roughness (Figure S4). XPS spectra confirmed the change in the chemical states on the HC-PEMs' surfaces by introducing an oxygen functional group (e.g., hydroxyl, carbonyl, carboxyl). Figure 2d shows the wide-scan XPS spectra of the reference, plasma-treated without etching, and plasma-etched HC-PEMs. Compared to the reference, the plasma-treated HC-PEMs showed an increase in the atomic ratio of oxygen (26.19 and 33.99 atom %, without etching and with etching, respectively), indicating that oxygen functional groups were introduced on the membrane surface through oxygen plasma treatment. The etching process can introduce further oxygen functional groups by enlarging the surface area due to increased micro-/nano roughness. For a deeper analysis, the C 1s spectra were deconvoluted for the reference and the modified HC-PEMs. As shown in Figure 2e, the modified membranes with plasma showed a distinct increase in carboxyl (−COOH) and hydroxyl (−OH) signals.[28−30] These results

https://doi.org/10.1021/acsami.2c15122
ACS Appl. Mater. Interfaces XXXX, XXX, XXX−XXX

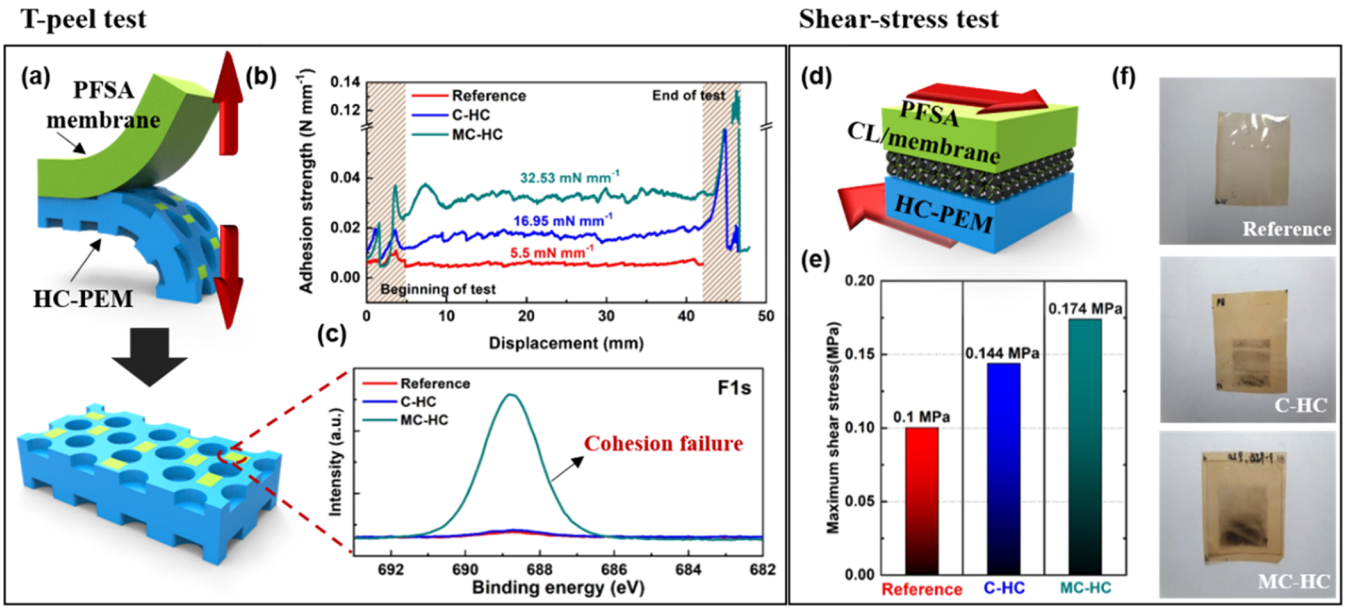

Figure 3. (a) Schematic of the T-peel test. (b) Peel-off strength between the perfluorosulfonic acid (PFSA) membrane (Nafion) and the hydrocarbon-based (HC) polymer electrolyte membranes (PEMs). (c) F1s spectra on the delaminated surface for the reference, chemically modified hydrocarbon (C-HC), and mechanically and chemically modified HC-based (MC-HC) membranes. (d) Schematic of the shear stress test. (e) Maximum shear stress between the PFSA electrode and the HC-PEM. (f) Digital images of the HC-PEM after shear stress test.

show that oxygen functional groups containing −OH and −COOH groups were introduced to the membrane surface, and the membrane surface was chemically activated with high surface energy via plasma treatment, consistent with the dramatic decrement of contact angle values of 79.5, 17.8, and 4.9° for the reference, C-HC, and MC-HC, respectively (Figure S5).

Before analyzing the effect of plasma treatment on the adhesive property and single-cell performance of the MEAs, the membrane basic properties of the pristine and modified HC-PEMs were investigated by performing proton conductivity measurements and mechanical tensile tests. Figure 2f shows the comparison of proton conductivity, and Table 1 summarizes the values of water uptake and swelling ratios (i.e., dimensional stability) for the reference, C-HC, and MC-HC, respectively.

From the comparable proton conductivities of the pristine and modified HC-PEMs, the surface modification using the plasma process to the HC-PEMs does not significantly affect the membrane's ion-transporting properties. In this study, all of the membranes (reference, C-HC, and MC-HC) were made of the polymer with the same structure and degree of sulfonation (40%). On the other hand, the samples prepared using the plasma process (C-HC and MC-HC) showed an increase in water uptake and dimensional swelling in the through-plane direction and a slight decrease in dimensional swelling in the in-plane direction. This is because the introduction of the oxygen functional groups on the membrane surface (C-HC and MC-HC) makes the wettability change of C-HC and MC-HC (Figure S5), and this accelerates the retention of water molecules at the membrane surface. Furthermore, from the measured mechanical properties of the membrane (Figure S6), the reference and C-HC show similar ultimate tensile strengths, Young's modulus, and elongation at the break. However, the MC-HC showed a little decrease in elongation at the break due to the stress concentration effect at the edges of the microsized structures.[31−33]

Next, two experiments were conducted to quantitatively compare the adhesion enhancement of the plasma-modified HC with a PFSA ionomer: (1) The T-peel test for laminates of the Reference/Nafion, C-HC/Nafion, and MC-HC/Nafion; (2) The shear stress measurement for laminates of the Reference/CL/Nafion, C-HC/CL/Nafion, and MC-HC/CL/Nafion. From Figure 3a, the T-peel test was performed by pulling the HC and commercial PFSA membranes (Nafion 212) in the opposite direction perpendicular to the laminates, like a T-shape. The strength was defined as the measured force normalized by the width of the laminates (Figure 3b).

Except for a sudden increase at the beginning and the end of the test, differences in the average peel-off strength were observed among the samples. While the Reference/Nafion showed a peeling strength of 5.5 mN mm^{-1}, the C-HC/Nafion and MC-HC/Nafion showed increased strengths of 16.95 mN mm^{-1} (~308% of the reference) and 32.53 mN mm^{-1} (~591% of the reference), respectively. The higher adhesion strength of the laminates with C-HC/Nafion than the reference/Nafion indicates a strong adhesion bonding at the interface due to oxygen functional group-induced hydrogen bonding and/or chemical bonding with condensation reactions.[28,34,35] Furthermore, it was confirmed that the laminates of the MC-HC/Nafion can have further enhanced adhesion properties due to the chemical effect of generating more oxygen functional groups and the mechanical fastener effect from microhole array-patterned geometry. Interestingly, by performing XPS measurements with the pristine and modified HC membranes from the samples after the T-peel tests, a strong F peak appeared on the MC-HC surface (Figure 3c). This cohesion failure occurred at the interface between the MC-HC and Nafion membranes (containing the F component), indicating that strong bonding adhesion between the MC-HC and the Nafion was formed. To evaluate the interface bonding strength for porous CL (Figure 3d), the shear stress was measured by holding the two membranes (HC and CL-coated Nafion) on different sides and pulling them in the opposite direction.

https://doi.org/10.1021/acsami.2c15122
ACS Appl. Mater. Interfaces XXXX, XXX, XXX−XXX

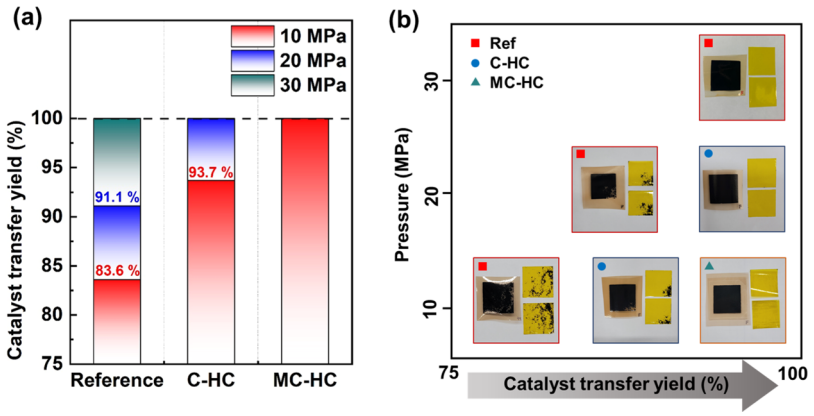

Figure 4. (a) Catalyst transfer yield according to the decal pressure for the reference, chemically modified hydrocarbon (C-HC), and mechanically and chemically modified HC-based (MC-HC) membranes. (b) Digital images of the fabricated membrane−electrode assembly (MEA) and residue decal films.

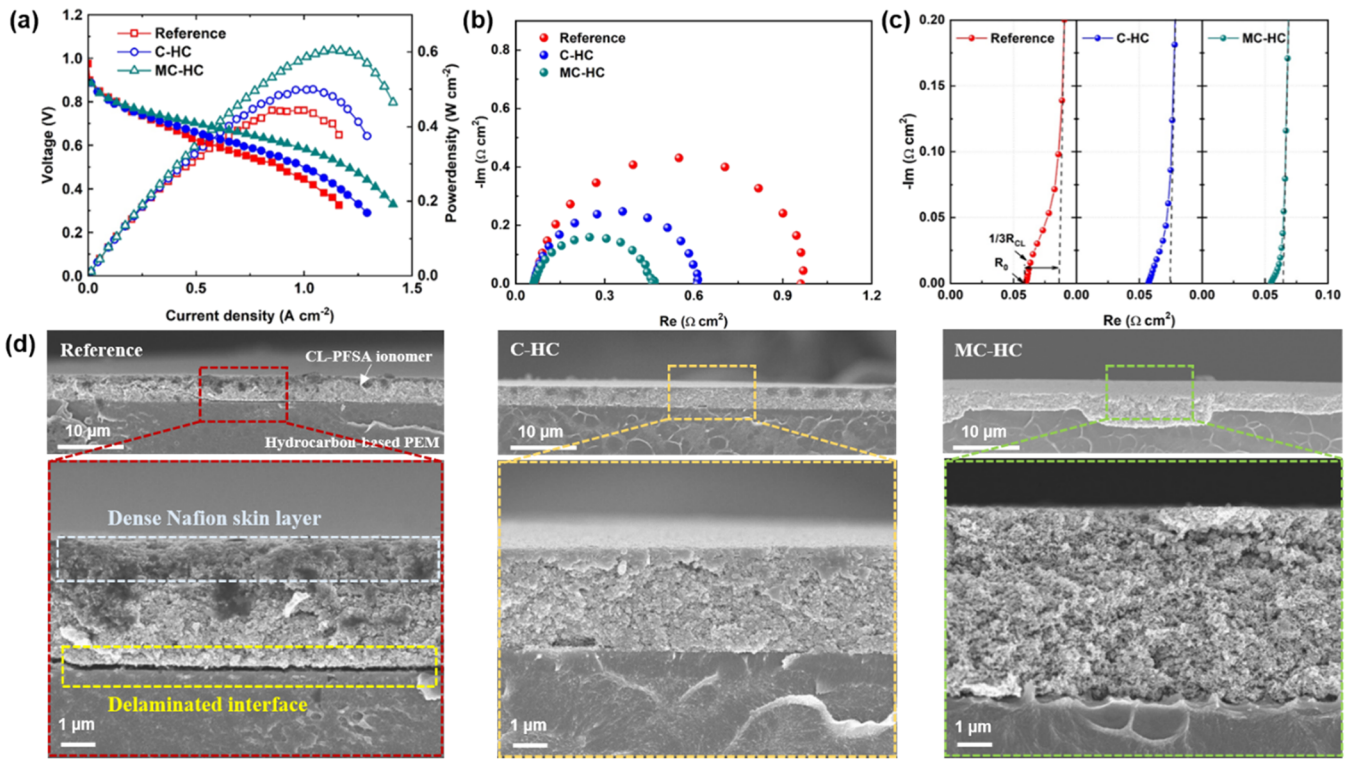

Figure 5. (a) Polarization curves at 80 °C, supplying fully humidified H_2 (150 sccm)/air (800 sccm) without back-pressure. (b) Corresponding electrochemical impedance spectra (EIS) at 0.6 V for the membrane−electrode assemblies (MEAs) with the reference, chemically modified hydrocarbon (C-HC), and mechanically and chemically modified HC-based (MC-HC) membranes. (c) EIS spectra obtained in the H_2/N_2 feed at 0.2 V. (d) Cross-sectional scanning electron microscopy (SEM) images of the MEAs with the reference, C-HC, and MC-HC.

Figure 3e shows the maximum shear stress of the prepared laminates. While the reference/CL showed maximum shear stress of ~0.1 MPa, the C-HC/CL (0.144 MPa) and MC-HC/CL (0.174 MPa) showed ~43 and ~74% increased shear stress, respectively. Furthermore, as shown by the digital camera image after the shear stress measurements (Figure 3f), residual CLs are attached to the C-HC and MC-HC surface, unlike the reference where the interface between the HC membrane and CL was neatly peeled off after the test. This result correlates with the previously observed T-peel test, indicating that the plasma-modified HC-PEM can improve adhesion between the PFSA membranes and the porous CL containing PFSA. This result is significant when applying the decal transfer method and analyzing the resistances within the MEAs. The decal transfer method with HC-PEMs requires a much higher temperature and/or pressure than the PFSA-based PEM due to its high glass-transition temperature (PFSA ~ 120 °C and HC > 200 °C),[36−38] high rigidity, and low compatibility with CL containing a PFSA ionomer. Therefore, performing the decal transfer method at low pressure and temperature by employing enhanced interfacial bonding properties can achieve advantages in the MEA manufacturing process and high-performance PEMFC with low-cost HC-PEMs.

Figure 4a shows the catalyst transfer yield according to the lamination pressures for the reference, C-HC, and MC-HC,

https://doi.org/10.1021/acsami.2c15122
ACS Appl. Mater. Interfaces XXXX, XXX, XXX−XXX

Table 2. Summary of Key Parameters from the Current−Voltage Curves and Electrochemical Impedance Spectra (EIS)

	polarization curve	EIS (H_2/N_2@0.2 V)		EIS (H_2/air@0.6 V)	cyclic voltammetry (CV)
samples	peak power density (PPD) (mW cm^{-2})	R_0 (Ω cm^2)	R_{CL}(Ω cm^2)	R_{LF-HF}(Ω cm^2)	ECSA (m^2 g_{pt}^{-1})
reference	450	0.05979	0.0822	0.9018	36.229
C-HC	504	0.05732	0.051	0.5519	37.135
MC-HC	606	0.05471	0.0306	0.3989	37.839

and Figure 4b shows the corresponding digital images of the resulting MEAs and PI films after delamination. The reference had the weakest bonding adhesion force between the membrane and the electrode and exhibited a lower transfer rate (83.6% at 10 MPa, 91.1% at 20 MPa, and completely transferred at 30 MPa) than C-HC and MC-HC. However, the C-HC showed a transfer rate of 93.7% at 10 MPa and was completely transferred at 20 MPa. The MC-HC was completely transferred at 10 MPa due to the strongest bonding adhesion strength through the plasma-etching process, which induced chemically activated high-energy surface and microhole array geometry.

For evaluating the electrochemical performances of the reference, C-HC, and MC-HC, the MEAs were fabricated under each optimized decal transfer condition at a constant temperature of 140 °C, with different applying pressures of 30, 20, and 10 MPa for the reference, C-HC, and MC-HC, respectively.

Figure 5a shows the polarization curves at 80 °C under the fully humidified condition by supplying H_2 (150 sccm)/Air (800 sccm). Compared to the peak power density (PPD) of the reference MEA (450 mW cm^{-2}), the modified MEAs with C-HC and MC-HC exhibited much higher PPDs of 504 and 606 mW cm^{-2}, increased by 12.0 and 34.7%, respectively. From the EIS spectra under the same operating condition at 0.6 V (Figure 5b), the smallest R_{LF-HF}, calculated from the semicircle radius and signifying the combined contribution of the charge-transfer and mass-transport resistances at the high current density region, was observed for the MEA with MC-HC (0.399 Ω cm^2) compared with that of the MEAs with the reference (0.902 Ω cm^2) and the C-HC (0.552 Ω cm^2). Because all MEAs used the same electrode and no difference occurs between the catalyst and the ionomer, this difference can be ascribed to the plasma-induced improved interfacial properties at the membrane/electrode interface and the modified electrode structure due to microhole patterns and different applying pressures during the decal process. EIS spectra were measured under H_2/N_2 atmosphere for a more detailed analysis, and a transmission line model was applied to interpret the results.[24,39−41] From the impedance response, an Ohmic resistance from the cell elements (R_0) and a protonic resistance across the catalyst layer (R_{CL}) can be defined. Because a deviation occurs between the ideal model and the actual spectra, this study defines the R_0 value as the intercept value of the spectrum and x-axis. From Figure 5c, the R_0 and R_{CL} values decrease in the order of the MEAs with the reference, C-HC, and MC-HC. Compared to the MEA with the reference (0.0598 Ω cm^2), MEAs with C-HC (0.0573 Ω cm^2) and MC-HC (0.0547 Ω cm^2) showed decreased R_0 of ∼4.2 and ∼8.5%, respectively.

Because reference and C-HC had the same membrane thickness, the decrease in R_0 was due to a decrease in the interface resistance between the membrane and CL. Additionally, the etching process-induced locally thinned membrane thickness of the MC-HC further reduced the R_0. A slightly increased hydrogen crossover density was observed for the MEAs with the MC-HC having a locally shortened path region (Figure S7); however, this value is still much smaller than that of a thick Nafion 212 membrane (e.g., 50 μm thickness). Notably, from the cross-sectional SEM images for the prepared MEAs, various morphological features of the membrane, the CL, and their interfaces are observed (Figure 5d). The MEAs with the reference PEM show severe delamination at the interface between the membrane and the CL and a notable PFSA ionomer (Nafion) skin layer on the CL outer surface. Therefore, the delamination due to low adhesion strength at the interface increases the R_0. Moreover, the MEAs with the reference (0.0822 Ω cm^2) significantly increased the R_{CL} compared with the MEAs with the modified membranes (0.051 and 0.0306 Ω cm^2 for MEAs with C-HC and MC-HC, respectively). The results show that the delamination at the interface restricted the proton transport to CL, causing an increase and inhomogeneity in R_{CL}.[24,41] However, the MEAs with C-HC and MC-HC had a tightly bonded interface due to plasma-induced improved bonding adhesion forces and showed much lower R_{CL} and R_0 (Table 2).

Primarily, for the MEAs with the MC-HC, the CL layer is conformally formed along the MC-HC shape by filling the microsized holes. This enlarged interfacial contact area provides extended proton transport pathways and improved compatibility between the HC-PEM and the CL, and lower laminating pressure results in better uniform ionomer distribution in the CLs compared with the reference MEAs. Next, by comparing each MEA's electrochemical active surface area (ECSA), the CV spectra were obtained (Figure S8), and the calculated ECSA values are summarized in Table 2. The ECSA of MEAs with the reference PEM was 36.23 m^2 g_{pt}^{-1}, whereas the MEAs with C-HC and MC-HC slightly increased by ∼2.6% (37.14 m^2 g_{pt}^{-1}) and ∼4.4% (37.84 m^2 g_{pt}^{-1}), respectively. The conformal contact between the membrane and the electrode and the enlarged surface area due to the micro- and nanosized structures caused this increase, but the differences were too small to affect the MEA performance.

After observing the current−voltage characteristics and the effect of reducing the protonic resistance with the modified MEAs, each MEA's limiting current density was measured using diluted oxygen gases and controlling back-pressures to analyze the significant reduction in the mass transfer resistance (R_{LF-HF}), showing the greatest effect on the performance. The total oxygen transport resistance (R_t) can be calculated using the following equation[42−44]

$$R_t = 4F\frac{X_{O_2}}{j_{lim}}\frac{P - P_W}{RT} \quad (5)$$

where F is the Faraday number, X_{O_2} is the oxygen mole fraction, j_{lim} is the limiting current density, P and P_W are total gas and water vapor pressures, respectively, R is the gas constant, and T is the cell temperature. Figure S9 shows the limiting current density for each mole fraction of the oxygen

https://doi.org/10.1021/acsami.2c15122
ACS Appl. Mater. Interfaces XXXX, XXX, XXX−XXX

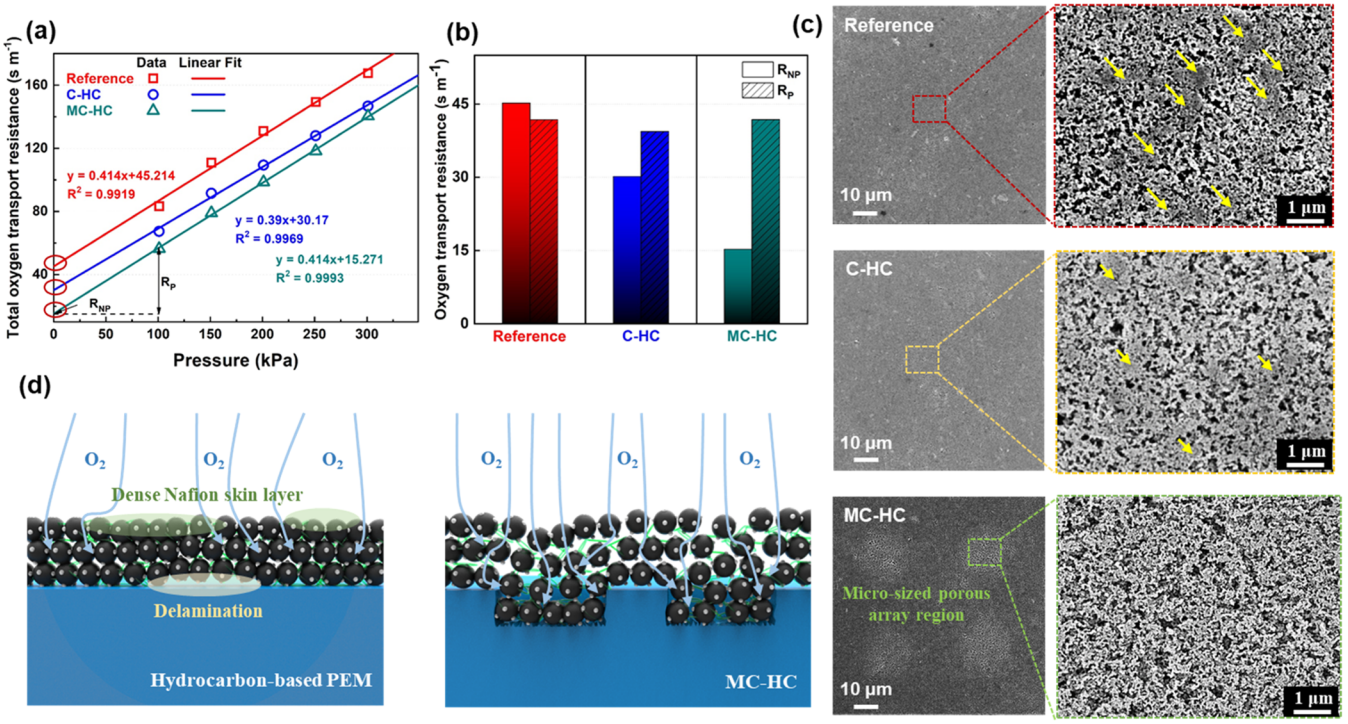

Figure 6. (a) Total oxygen transport resistance of membrane−electrode assemblies (MEAs) with the reference, chemically modified hydrocarbon (C-HC), and mechanically and chemically modified HC-based (MC-HC) membranes according to the pressure. (b) Pressure-independent and pressure-dependent oxygen transport resistances (at 101 kPa) from (a). (c) Surface scanning electron microscopy (SEM) images of MEAs with the reference, C-HC, and MC-HC. (d) Schematic illustrations of MEAs with pristine and MC-HC polymer electrolyte membranes (PEMs).

and total gas pressures for the samples with the reference, C-HC, and MC-HC. The ratio of X_{O_2} and j_{lim} (i.e., slope) was obtained by fitting the regression straight line passing through the origin for each pressure. Then, the linear relationship between the total oxygen transport resistance and the total gas pressure can be graphically represented (Figure 6a). From the graph, the contribution of pressure-dependent (R_P, at channel and GDL) and pressure-independent (R_{NP}, at CL and ionomer film) oxygen transport resistances to R_t can be separately obtained through the linear trend line of R_t.

Figure 6b shows the calculated R_P and R_{NP} for the prepared samples. Because the same flow channels and GDLs were used, all samples showed similar R_P values, affected by the flow channel geometry and macropore distribution of GDL. However, for R_{NP}, the samples with C-HC and MC-HC show 33% (30.30 s m^{-1}) and 65.23% (15.72 s m^{-1}) decreased values compared with the reference (45.214 s m^{-1}). The morphological characteristics of the CLs for each MEA were analyzed using SEM measurement to find the reason for the reduced oxygen transport resistance in the CL (Figure 6c). For the CL on the reference PEM, a severe Nafion skin layer was observed on the CL surface where the CL and GDL contact, restricting the oxygen transport to the CL. It was also observed in the cross-sectional image of the CL (Figure 5d). However, for C-HC, the formation of the Nafion skin layer was alleviated, indicating that a decrease in decal pressure reduces the Nafion skin layer outside CL.[45] Here, for MC-HC and the alleviation of the Nafion skin layer, a highly porous area was formed along the microsized hole array region. This highly porous patterned region can provide an oxygen transport highway into the CL, explaining the significant decrease in the oxygen transfer resistance-induced improved mass-transport capacity for MEAs with MC-HC. Figure 6d shows the effect of this oxygen plasma-mediated microstructured HC-PEM for improving mass transport.

4. CONCLUSIONS

In summary, we proposed a novel mechanical and chemical modification technique for an HC membrane to improve the interface adhesion and mass-transport capacity in PEMFCs. Microsized holes and oxygen functional groups were successfully introduced onto the HC membrane's surface through an oxygen plasma process with a polymer stencil with regular openings. This modified HC membrane enabled low-pressure and low-temperature decal transfer, allowing a highly porous patterned electrode region that can provide an oxygen transport highway. The MEAs with a modified HC membrane exhibited much higher PEMFC performance than the reference MEAs. The physical, chemical, and electrochemical characteristics of the modified HC membrane and the MEA were extensively investigated. This simple modification technique for HC-based membranes could contribute to the research fields of high-efficiency and low-cost PEMFCs using HC-PEM and to other electrochemical devices that require improved interface compatibilities, such as battery and water electrolysis systems.

■ ASSOCIATED CONTENT

Supporting Information

The Supporting Information is available free of charge at https://pubs.acs.org/doi/10.1021/acsami.2c15122.

Diagram of the fabrication process of a polymeric stencil (Figure S1); SEM images of a plasma-etched BPSH-40 membrane (Figure S2); chemical structure of BPSH-40

https://doi.org/10.1021/acsami.2c15122
ACS Appl. Mater. Interfaces XXXX, XXX, XXX−XXX

(Figure S3); cross-sectional SEM images of MC-HC and high-magnification SEM images (Figure S4); water contact angle on the reference, chemically modified hydrocarbon (C-HC), and mechanically and chemically modified HC-based (MC-HC) membranes (Figure S5); stress−strain curves of the reference, chemically modified hydrocarbon (C-HC), and mechanically and chemically modified HC-based (MC-HC) membranes (Figure S6); linear sweep voltammetry spectra of the reference, chemically modified hydrocarbon (C-HC), and mechanically and chemically modified HC-based (MC-HC) membranes (Figure S7); cyclic voltammetry (CV) spectra of the reference, chemically modified hydrocarbon (C-HC), and mechanically and chemically modified HC-based (MC-HC) membranes (Figure S8); and limiting current densities of the reference, chemically modified hydrocarbon (C-HC), and mechanically and chemically modified HC-based (MC-HC) membranes according to the oxygen mole faction and pressure (Figure S9) (PDF)

AUTHOR INFORMATION

Corresponding Authors

Hyoung-Juhn Kim − *Hydrogen Energy Technology Laboratory, Korea Institute of Energy Technology (KENTECH), Naju, Jeonnam 58330, Republic of Korea*; Email: hjk@kentech.ac.kr

Mansoo Choi − *Global Frontier Center for Multiscale Energy Systems, Seoul National University, Seoul 08826, Republic of Korea; Department of Mechanical Engineering, Seoul National University, Seoul 08826, Republic of Korea*; orcid.org/0000-0003-3198-6899; Email: mchoi@snu.ac.kr

Segeun Jang − *Department of Mechanical Engineering, Kookmin National University, Seoul 02707, Republic of Korea*; orcid.org/0000-0001-8319-8400; Email: sjang@kookmin.ac.kr

Authors

Jiwoo Choi − *Global Frontier Center for Multiscale Energy Systems, Seoul National University, Seoul 08826, Republic of Korea; Department of Mechanical Engineering, Seoul National University, Seoul 08826, Republic of Korea*

Dongsu Kim − *Department of Mechanical Engineering, Kookmin National University, Seoul 02707, Republic of Korea*

Ji Eon Chae − *Department of Mobility Power Research, Korea Institute of Machinery & Materials, Yuseong-gu, Daejeon 34103, Korea*

Sanghyeok Lee − *Department of Mechanical Engineering, Kookmin National University, Seoul 02707, Republic of Korea*

Sang Moon Kim − *Department of Mechanical Engineering, Incheon National University, Incheon 22012, Republic of Korea*; orcid.org/0000-0002-2311-2211

Sung Jong Yoo − *Center for Hydrogen & Fuel Cell Research, Korea Institute of Science and Technology, Seoul 02792, Korea*; orcid.org/0000-0003-1556-0206

Complete contact information is available at: https://pubs.acs.org/10.1021/acsami.2c15122

Author Contributions

○J.C., D.K., and J.E.C. contributed equally to this work.

Notes

The authors declare no competing financial interest.

ACKNOWLEDGMENTS

This work was funded by the Global Frontier R&D Program of the Center for Multiscale Energy Systems funded by the NRF, Korea (NRF-2019R1C1C1005258), and Korea Electric Power Corporation (grant no. R21XO01-27)

REFERENCES

(1) Yee, R. S. L.; Rozendal, R. A.; Zhang, K.; Ladewig, B. P. Cost Effective Cation Exchange Membranes: A Review. *Chem. Eng. Res. Des.* **2012**, *90*, 950−959.

(2) Nguyen, H. L.; Han, J.; Nguyen, X. L.; Yu, S.; Goo, Y.-M.; Le, D. D. Review of the Durability of Polymer Electrolyte Membrane Fuel Cell in Long-Term Operation: Main Influencing Parameters and Testing Protocols. *Energies* **2021**, *14*, 4048.

(3) Wang, L.; Wan, X.; Liu, S.; Xu, L.; Shui, J. Fe-N-C Catalysts for Pemfc: Progress Towards the Commercial Application under Doe Reference. *J. Energy Chem.* **2019**, *39*, 77−87.

(4) Zatoń, M.; Rozière, J.; Jones, D. J. Current Understanding of Chemical Degradation Mechanisms of Perfluorosulfonic Acid Membranes and Their Mitigation Strategies: A Review. *Sustainable Energy Fuels* **2017**, *1*, 409−438.

(5) Du, S. Recent Advances in Electrode Design Based on One-Dimensional Nanostructure Arrays for Proton Exchange Membrane Fuel Cell Applications. *Engineering* **2021**, *7*, 33−49.

(6) Ahmad, S.; Nawaz, T.; Ali, A.; Orhan, M. F.; Samreen, A.; Kannan, A. M. An Overview of Proton Exchange Membranes for Fuel Cells: Materials and Manufacturing. *Int. J. Hydrogen Energy* **2022**, *47*, 19086−19131.

(7) Rui, Z.; Liu, J. Understanding of Free Radical Scavengers Used in Highly Durable Proton Exchange Membranes. *Prog. Nat. Sci.: Mater. Int.* **2020**, *30*, 732−742.

(8) Kim, K.; Heo, P.; Hwang, W.; Baik, J. H.; Sung, Y. E.; Lee, J. C. Cross-Linked Sulfonated Poly(Arylene Ether Sulfone) Containing a Flexible and Hydrophobic Bishydroxy Perfluoropolyether Cross-Linker for High-Performance Proton Exchange Membrane. *ACS Appl. Mater. Interfaces* **2018**, *10*, 21788−21793.

(9) Kumar, A. G.; Singh, A.; Komber, H.; Voit, B.; Tiwari, B. R.; Noori, M. T.; Ghangrekar, M. M.; Banerjee, S. Novel Sulfonated Co-Poly(Ether Imide)S Containing Trifluoromethyl, Fluorenyl and Hydroxyl Groups for Enhanced Proton Exchange Membrane Properties: Application in Microbial Fuel Cell. *ACS Appl. Mater. Interfaces* **2018**, *10*, 14803−14817.

(10) Wang, L.; Deng, N.; Wang, G.; Ju, J.; Cheng, B.; Kang, W. Constructing Amino-Functionalized Flower-Like Metal-Organic Framework Nanofibers in Sulfonated Poly(Ether Sulfone) Proton Exchange Membrane for Simultaneously Enhancing Interface Compatibility and Proton Conduction. *ACS Appl. Mater. Interfaces* **2019**, *11*, 39979−39990.

(11) Parnian, M. J.; Rowshanzamir, S.; Prasad, A. K.; Advani, S. G. High Durability Sulfonated Poly (Ether Ether ketone)-Ceria Nanocomposite Membranes for Proton Exchange Membrane Fuel Cell Applications. *J. Membr. Sci.* **2018**, *556*, 12−22.

(12) Date, B.; Han, J.; Park, S.; Park, E. J.; Shin, D.; Ryu, C. Y.; Bae, C. Synthesis and Morphology Study of Sebs Triblock Copolymers Functionalized with Sulfonate and Phosphonate Groups for Proton Exchange Membrane Fuel Cells. *Macromolecules* **2018**, *51*, 1020−1030.

(13) Higashihara, T.; Matsumoto, K.; Ueda, M. Sulfonated Aromatic Hydrocarbon Polymers as Proton Exchange Membranes for Fuel Cells. *Polymer* **2009**, *50*, 5341−5357.

(14) Zhu, H. Speek Scaling Up. *Joule* **2022**, *6*, 718−720.

(15) Pu, X.; Duan, Y.; Li, J.; Ru, C.; Zhao, C. Understanding of Hydrocarbon Ionomers in Catalyst Layers for Enhancing the Performance and Durability of Proton Exchange Membrane Fuel Cells. *J. Power Sources* **2021**, *493*, No. 229671.
(16) Long, Z.; Miyake, J.; Miyatake, K. Partially Fluorinated Polyphenylene Ionomers as Proton Exchange Membranes for Fuel Cells: Effect of Pendant Multi-Sulfophenylene Groups. *ACS Appl. Energy Mater.* **2019**, *2*, 7527−7534.
(17) Bi, C.; Zhang, H.; Xiao, S.; Zhang, Y.; Mai, Z.; Li, X. Grafted Porous Ptfe/Partially Fluorinated Sulfonated Poly(Arylene Ether Ketone) Composite Membrane for Pemfc Applications. *J. Membr. Sci.* **2011**, *376*, 170−178.
(18) Sankir, M.; Kim, Y. S.; Pivovar, B. S.; McGrath, J. E. Proton Exchange Membrane for Dmfc and H2/Air Fuel Cells: Synthesis and Characterization of Partially Fluorinated Disulfonated Poly(Arylene Ether Benzonitrile) Copolymers. *J. Membr. Sci.* **2007**, *299*, 8−18.
(19) Balogun, E.; Mardle, P.; Nguyen, H.; Breitwieser, M.; Holdcroft, S. Catalyst Layers for Fluorine-Free Hydrocarbon Pemfcs. *Electrochim. Acta* **2022**, *401*, No. 139479.
(20) Chae, J. E.; Yoo, S. J.; Kim, J. Y.; Jang, J. H.; Lee, S. Y.; Song, K. H.; Kim, H.-J. Hydrocarbon-Based Electrode Ionomer for Proton Exchange Membrane Fuel Cells. *Int. J. Hydrogen Energy* **2020**, *45*, 32856−32864.
(21) Jeong, H. Y.; Yang, D.-S.; Han, J. H.; Lee, J. Y.; So, S.; Suh, D. H.; Hong, S. K.; Hong, Y. T.; Kim, T.-H. Novel Interfacial Bonding Layers with Controlled Gradient Composition Profile for Hydrocarbon-Based Membrane Electrode Assemblies. *J. Power Sources* **2018**, *398*, 1−8.
(22) Nam, S.-W.; Yu, D. M.; Kim, T.-H.; Lee, J. Y.; Nam, S. Y.; Hong, Y. T. Synthesis and Properties of Bonding Layer Containing Flexible and Fluorinated Moieties for Hydrocarbon-Based Membrane Electrode Assemblies. *Int. J. Hydrogen Energy* **2016**, *41*, 10884−10895.
(23) Oh, K.-H.; Bae, I. Engineered Membrane−Electrode Interface for Hydrocarbon-Based Polymer-Electrolyte-Membrane Fuel Cells Via Solvent-Vapor-Annealed Deposition. *ACS Appl. Nano Mater.* **2019**, *2*, 3857−3863.
(24) Oh, K. H.; Kang, H. S.; Choo, M. J.; Jang, D. H.; Lee, D.; Lee, D. G.; Kim, T. H.; Hong, Y. T.; Park, J. K.; Kim, H. T. Interlocking Membrane/Catalyst Layer Interface for High Mechanical Robustness of Hydrocarbon-Membrane-Based Polymer Electrolyte Membrane Fuel Cells. *Adv. Mater.* **2015**, *27*, 2974−2980.
(25) Yuk, S.; Yuk, J.; Kim, T.-H.; Hong, Y. T.; Lee, D.-H.; Hyun, J.; Choi, S.; Doo, G.; Lee, D. W.; Kim, H.-T. External Reinforcement of Hydrocarbon Membranes by a Three-Dimensional Interlocking Interface for Mechanically Durable Polymer Electrolyte Membrane Fuel Cells. *J. Power Sources* **2019**, *415*, 44−49.
(26) Cho, H.; Kim, S. M.; Kang, Y. S.; Kim, J.; Jang, S.; Kim, M.; Park, H.; Bang, J. W.; Seo, S.; Suh, K.-Y.; Sung, Y.-E.; Choi, M. Multiplex Lithography for Multilevel Multiscale Architectures and Its Application to Polymer Electrolyte Membrane Fuel Cell. *Nat. Commun.* **2015**, *6*, No. 8484.
(27) Choi, E.; Kim, S. M.; Jang, S. Highly Durable Membrane Electrode Assembly with Multiwalled Carbon Nanotubes/Ceo2-Reinforced Nafion Composite Membrane by Spraying Method for Fuel Cell Applications. *Adv. Mater. Technol.* **2022**, *7*, No. 2101360.
(28) Endo, T.; Reddy, L.; Nishikawa, H.; Kaneko, S.; Nakamura, Y.; Endo, K. Composite Engineering − Direct Bonding of Plastic Pet Films by Plasma Irradiation. *Procedia Eng.* **2017**, *171*, 88−103.
(29) Ma, W.; Panecka, M.; Tufenkji, N.; Rahaman, M. S. Bacteriophage-Based Strategies for Biofouling Control in Ultrafiltration: In Situ Biofouling Mitigation, Biocidal Additives and Biofilm Cleanser. *J. Colloid Interface Sci.* **2018**, *523*, 254−265.
(30) Zhang, L.; Tu, L. Y.; Liang, Y.; Chen, Q.; Li, Z. S.; Li, C. H.; Wang, Z. H.; Li, W. Coconut-Based Activated Carbon Fibers for Efficient Adsorption of Various Organic Dyes. *RSC Adv.* **2018**, *8*, 42280−42291.
(31) Seol, C.; Jang, S.; Lee, J.; Nam, L. V.; Pham, T. A.; Koo, S.; Kim, K.; Jang, J.-H.; Kim, S. M.; Yoo, S. J. High-performance fuel cells with a plasma-etched polymer electrolyte membrane with microhole arrays. *ACS Sustainable Chem. Eng.* **2021**, *9*, 5884−5894.
(32) Ahn, C. Y.; Jang, S.; Cho, Y. H.; Choi, J.; Kim, S.; Kim, S. M.; Sung, Y.-E.; Choi, M. Guided cracking of electrodes by stretching prism-patterned membrane electrode assemblies for high-performance fuel cells. *Sci. Rep.* **2018**, *8*, No. 1257.
(33) Kráčalík, M. Effect Of A Surface Roughness On The Crack Driving Force Of Physically Short Stationary Crack−Numerical Simulation. *Acta Simul.* **2018**, *4*, 7−10.
(34) Ohkubo, Y.; Endo, K.; Yamamura, K. Adhesive-Free Adhesion between Heat-Assisted Plasma-Treated Fluoropolymers (Ptfe, Pfa) and Plasma-Jet-Treated Polydimethylsiloxane (Pdms) and Its Application. *Sci. Rep.* **2018**, *8*, No. 18058.
(35) Ohkubo, Y.; Ishihara, K.; Shibahara, M.; Nagatani, A.; Honda, K.; Endo, K.; Yamamura, K. Drastic Improvement in Adhesion Property of Polytetrafluoroethylene (Ptfe) Via Heat-Assisted Plasma Treatment Using a Heater. *Sci. Rep.* **2017**, *7*, No. 9476.
(36) Jung, H.-Y.; Kim, J. W. Role of the Glass Transition Temperature of Nafion 117 Membrane in the Preparation of the Membrane Electrode Assembly in a Direct Methanol Fuel Cell (Dmfc). *Int. J. Hydrogen Energy* **2012**, *37*, 12580−12585.
(37) Choi, J.; Kyeong, M.; Kim, M.; Lee, S.-S.; Seo, B.; Park, H. S.; Park, H.-Y.; Henkensmeier, D.; Lee, S. Y.; Kim, H.-J. Synthesis of Sulfonated Poly(Arylene Ether Sulfone)S Containing Aliphatic Moieties for Effective Membrane Electrode Assembly Fabrication by Low-Temperature Decal Transfer Methods. *Polymers* **2021**, *13*, 11.
(38) Sulaiman, R. R. R.; Walvekar, R.; Khalid, M.; Wong, W. Y.; Jagadish, P. Recent Progress in the Development of Aromatic Polymer-Based Proton Exchange Membranes for Fuel Cell Applications. *Polymers* **2020**, *12*, 1061.
(39) Li, G.; Pickup, P. G. Ionic Conductivity of Pemfc Electrodes. *J. Electrochem. Soc.* **2003**, *150*, C745−C752.
(40) Lefebvre, M. C.; Martin, R. B.; Pickup, P. G. Characterization of Ionic Conductivity Profiles within Proton Exchange Membraen Fuel Cell Gas Diffusion Electrodes by Impedance Spectroscopy. *Electrochem. Solid-State Lett.* **1999**, *2*, 259−261.
(41) Malevich, D.; Jayasankar, B. R.; Halliop, E.; Pharoah, J. G.; Peppley, B. A.; Karan, K. On the Determination of Pem Fuel Cell Catalyst Layer Resistance from Impedance Measurement in H2/N2cells. *J. Electrochem. Soc.* **2012**, *159*, F888−F895.
(42) Kabir, S.; Myers, D. J.; Kariuki, N.; Park, J.; Wang, G.; Baker, A.; Macauley, N.; Mukundan, R.; More, K. L.; Neyerlin, K. C. Elucidating the Dynamic Nature of Fuel Cell Electrodes as a Function of Conditioning: An Ex Situ Material Characterization and in Situ Electrochemical Diagnostic Study. *ACS Appl. Mater. Interfaces* **2019**, *11*, 45016−45030.
(43) Wan, Z. H.; Zhong, Q.; Liu, S. F.; Jin, A. P.; Chen, Y. N.; Tan, J. T.; Pan, M. Determination of Oxygen Transport Resistance in Gas Diffusion Layer for Polymer Electrolyte Fuel Cells. *Int. J. Energy Res.* **2018**, *42*, 2225−2233.
(44) Baker, D. R.; Caulk, D. A.; Neyerlin, K. C.; Murphy, M. W. Measurement of Oxygen Transport Resistance in Pem Fuel Cells by Limiting Current Methods. *J. Electrochem. Soc.* **2009**, *156*, B991−B1003.
(45) Liang, X.; Pan, G.; Xu, L.; Wang, J. A Modified Decal Method for Preparing the Membrane Electrode Assembly of Proton Exchange Membrane Fuel Cells. *Fuel* **2015**, *139*, 393−400.

https://doi.org/10.1021/acsami.2c15122
ACS Appl. Mater. Interfaces XXXX, XXX, XXX−XXX